TCAD-Based Analysis on the Impact of AlN Interlayer in Normally-off AlGaN/GaN MISHEMTs with Buried p-Region

Saleem Hamady, Bilal Beydoun, Frédéric Morancho

electronics

MDPI

Article

TCAD-Based Analysis on the Impact of AlN Interlayer in Normally-off AlGaN/GaN MISHEMTs with Buried p-Region

Saleem Hamady [1,*], Bilal Beydoun [2,3] and Frédéric Morancho [4]

[1] College of Engineering and Technology, American University of the Middle East, Egaila 54200, Kuwait
[2] Laboratoire SATIE ENS Paris Saclay, Campus de Versailles-Satory, 25, Allée des Marronniers, 78000 Versailles, France; bbeydoun@cesi.fr
[3] CESI Ecole d'Ingénieur, Campus CESI Nanterre, 93 Boulevard de la Seine CS 40177, 92023 Nanterre Cedex, France
[4] Laboratoire d'Analyse et d'Architecture des Systèmes (LAAS-CNRS), Université de Toulouse, CNRS, UPS, 31031 Toulouse, France; morancho@laas.fr
* Correspondence: saleem.hamady@aum.edu.kw

Abstract: With the growing demand for more efficient power conversion and silicon reaching its theoretical limit, wide bandgap semiconductor devices are emerging as a potential solution. For instance, Gallium Nitride (GaN)-based high-electron-mobility transistors (HEMTs) are getting more attention, and several structures for the normally off operation have been proposed. Adding an AlN interlayer in conventional AlGaN/GaN normally on HEMT structures is known to enhance the current density. In this work, the effect of an AlN interlayer in the normally off AlGaN/GaN MISHEMT with a buried p-region was investigated using a TCAD simulation from Silvaco. The added AlN interlayer increases the two-dimensional electron gas density, requiring a higher p-doping concentration to achieve the same threshold voltage. The simulation results show that the overall effect is a reduction in the device's current density and peak transconductance by 21.83% and 44.4%, respectively. Further analysis of the current profile shows that because of the buried p-region and at high gate voltages, the current flows near the AlGaN/GaN interface and along the insulator/AlGaN interface. Adding an AlN interface blocks the migration of channel electrons to the insulator/AlGaN interface, resulting in a lower current density.

Keywords: gallium nitride (GaN); HEMT; TCAD simulation; Silvaco; AlN interlayer; buried p-region; wide bandgap

Academic Editors: Ray-Hua Horng, Yahya M. Meziani and Nakkeeran Kaliyaperumal

Received: 17 October 2024
Revised: 2 January 2025
Accepted: 10 January 2025
Published: 14 January 2025

Citation: Hamady, S.; Beydoun, B.; Morancho, F. TCAD-Based Analysis on the Impact of AlN Interlayer in Normally-off AlGaN/GaN MISHEMTs with Buried p-Region. *Electronics* **2025**, *14*, 313. https://doi.org/10.3390/electronics14020313

1. Introduction

Silicon has been the dominant material in power electronics for decades due to its well-understood properties and widespread availability [1–3]. However, with increasing power demands from applications like electric vehicles and renewable energy systems, silicon is now reaching its physical limits in terms of efficiency, thermal management, and switching speed [4–6]. Wide-bandgap (WBG) materials such as Gallium Nitride (GaN) and Silicon Carbide (SiC) present promising solutions to these challenges [7–10].

GaN-based devices, such as high-electron-mobility transistors (HEMTs), are particularly promising for high-frequency, high-power, and low-loss applications. These devices utilize GaN's polarization field to form a conductive channel. The polarization discontinuity at the heterointerface between GaN and AlGaN induces bound charges, attracting free electrons to form a two-dimensional electron gas (2DEG), enabling highly efficient electron transport [11–13]. This mechanism with the superior properties of GaN allows

GaN HEMTs to achieve higher breakdown voltages, greater thermal conductivity, and faster switching speeds than traditional silicon devices [14–17].

1.1. Normally off HEMTs

Conventional GaN HEMTs are normally on [18], operating in depletion mode, which means that current flows between the source and drain terminals at zero gate voltage (V_{gs} = 0 V). To block this current flow and turn the device off, a negative gate voltage must be applied. Power-switching applications necessitate devices exhibiting normally off characteristics due to fundamental safety and power efficiency requirements [19]. Achieving normally off GaN HEMTs has become a crucial research focus, with several methods proposed.

A widely explored method involves reducing the distance between the gate and the AlGaN/GaN interface. This can be accomplished by employing a thin barrier layer, which effectively minimizes the gate to AlGaN/GaN distance and facilitates normally off operation, as shown in studies [20–23]. Another approach is gate recessing, where selective etching of the barrier layer directly beneath the gate electrode is performed to achieve closer proximity to the interface. This technique is also well-documented in research efforts [24–27].

Alternative methods focus on conduction band engineering, which involves manipulating the energy bands within semiconductor devices to achieve specific electrical properties. In AlGaN/GaN heterostructures, positive charges at the AlGaN/GaN interface pull the conduction band below the Fermi level, resulting in the formation of a two-dimensional electron gas (2DEG) that serves as the device's channel. To realize normally off (enhancement-mode) operation, it is essential to deplete this 2DEG at zero gate voltage. This requires lifting the conduction band above the Fermi level at the interface. One way to achieve this is by introducing fluorine ions [28–31] or adding a p-type GaN layer [32–35] near the AlGaN/GaN interface. These additions raise the conduction band in that region, effectively depleting the 2DEG channel and enabling the desired normally off behavior. Although both fluorine ions and the p-GaN layer increase the energy gap between the conduction band and the Fermi level, an additional factor plays a key role in the p-GaN layer method. The discontinuity in the polarization field between the p-GaN and AlGaN layers creates a fixed negative bound charge at their interface. This results in a further shift in the conduction band. Although the p-region is usually placed above the AlGaN layer, a recent study has proposed achieving the normally off operation by burying a p-region below the AlGaN/GaN interface, specifically beneath the gate electrode [36]. The technique was experimentally validated in the work undertaken by [37]

1.2. Aluminum Nitride in GaN HEMTs

In GaN HEMTs, incorporating an Aluminum Nitride (AlN) layer has been reported to offer numerous advantages. In the work by [38], AlN was used to enhance device reliability and reduce gate leakage by forming double-barrier structures that mitigate electric field stress. Additionally, the work by [39] demonstrates record-high output power density at the X-band in HEMTs on free-standing AlN substrates, highlighting the significant potential of these devices as next-generation high-power radio frequency components. Moreover, the implementation of an AlN back barrier in conjunction with a thin, unintentionally-doped (UID) GaN channel demonstrated an absence of harmful impurity levels associated with current collapse phenomena [40]. When used as an interlayer between the barrier and the buffer layer, due to the high polarization field in the AlN layers compared to relaxed GaN layers, a high positive bound charge is created at the interface between the two layers. This significantly improves the density of the 2DEG, which will be reflected

in the current density and transconductance of the device [41–45]. While the addition of an AlN interlayer in conventional normally on HEMTs has been extensively studied and shown to offer significant advantages in terms of reducing gate leakage, increasing the current density, and enhancing transconductance, its effectiveness in normally off HEMTs incorporating a buried p-region remains unexamined.

Research Question: For normally off GaN HEMTs with a buried p-region, how does the inclusion of an AlN interlayer affect device performance when the threshold voltage is fixed? Specifically, will it increase the current density and transconductance of the device?

In this study, we aimed to answer this question using a TCAD simulation tool from Silvaco (atlas version 5.28.1.R).

2. Materials and Methods

Technology Computer-Aided Design (TCAD) tools are vital in the semiconductor industry. When properly calibrated, the tools can accurately predict the characteristics of electronic devices under different conditions. This capability accelerates the overall development timeline and reduces physical prototyping and iterative testing costs. Additionally, these tools offer more insight into the physics behind the operation of the simulated device, enabling further design/process optimization.

To ensure accurate and reliable simulation results, the following steps were adopted: First, to ensure accuracy, we began by calibrating the simulator using a conventional GaN HEMT (Section 2.1). This involved comparing the simulated electrical characteristics to experimental data of a reference device, ensuring that key metrics, like current density, threshold voltage, and transconductance, closely matched the experimental results. Next, we introduced the AlN interlayer into the simulated GaN HEMT structure. The aim was to validate the simulator's ability to replicate the performance improvements documented in the literature, particularly focusing on enhancements in current density and transconductance (Section 3.1). Likewise, a buried p-region was then integrated into the GaN HEMT structure to confirm that the model can accurately capture the intended threshold voltage shift toward more positive values, effectively transitioning the device to a normally off state (Section 3.2). Finally, both the AlN interlayer and the buried p-region were combined within the simulated device to assess whether the benefits observed from the AlN interlayer in conventional HEMTs, such as increased current density and transconductance, still hold in this modified normally off configuration. Specifically, we investigated if these benefits are maintained under a fixed threshold voltage (Section 3.3).

2.1. Simulation Calibration

The device simulator was calibrated using experimental electrical characteristics obtained from a normally on HEMT, as shown in Figure 1a. Critical physical parameters, including 2DEG density, acceptor trap energy levels, and acceptor trap density, were systematically adjusted during the calibration process. The resultant $I_d(V_{gs})$ transfer characteristics demonstrate excellent agreement between the simulated and experimental data, as shown in Figure 1b. The comprehensive parameter set employed for simulator calibration is detailed in [36].

2.2. The Simulated Structure

The simulated device structure is shown in Figure 2. The substrate layer is composed of silicon material and has a thickness of 0.5 µm. A GaN buffer layer of 1 µm was deposited on the substrate, followed by a 100 nm p-GaN layer. In this p-GaN layer, N doping was performed by excluding a region below the gate electrode. Subsequently, a 5 nm GaN layer was deposited; the region hosts the two-dimensional electron gas that acts as the

device's channel. Finally, a 25 nm $Al_{0.15}GaN$ layer was deposited to create the necessary polarization fields that confine the electrons in the 2DEG region. A thin layer of Si_3N_4 with a thickness of 10 nm was used and was covered by the gate electrode.

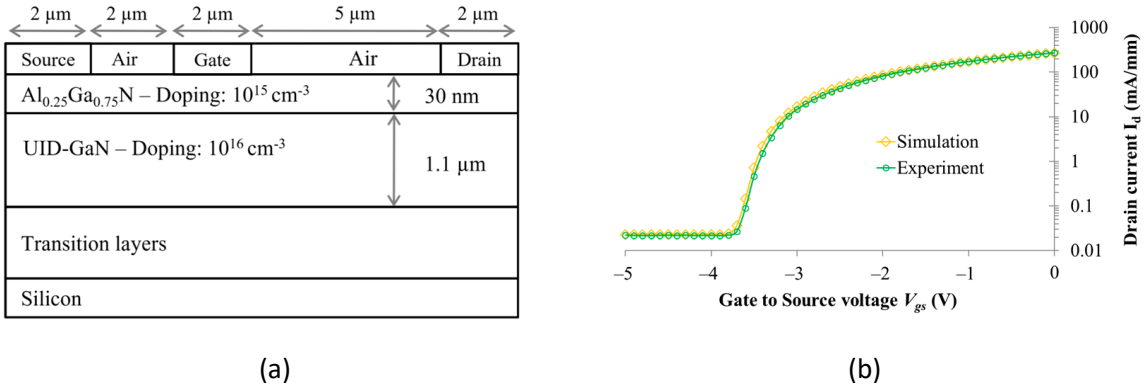

Figure 1. (**a**) Schematic cross-section of the normally on HEMT device used for calibration. (**b**) A comparison of experimental and simulated $I_d(V_{gs})$ transfer characteristics shows a clear match [36].

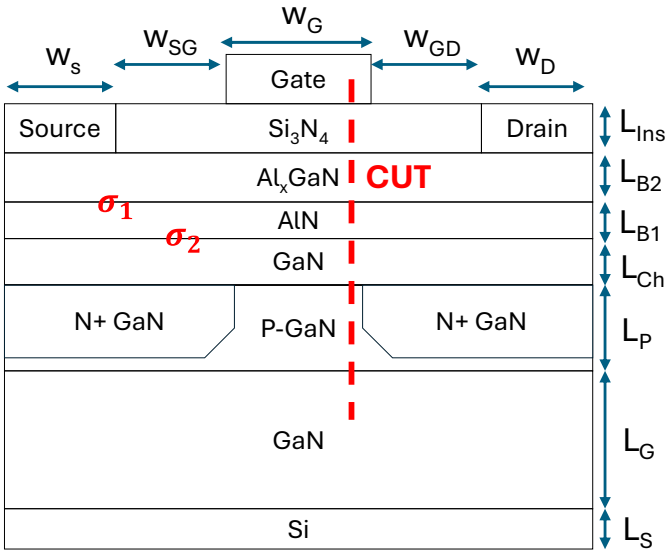

Figure 2. Normally off HEMT with a buried p-region and an AlN interlayer.

When simulating the effect of the AlN interlayer, the 25 nm AlGaN was replaced with a 2 nm AlN interlayer and a 23 nm AlGaN. The aim was to keep the gate at the same distance from the AlGaN/GaN interface (25 nm) to properly address the effect of the interlayer.

Regarding the lateral dimensions, the device length is 13 µm, divided as follows: 2 µm is the length of all electrodes (the source, gate, and drain). The distance between the source and the gate is 2 µm and between the gate and the drain is 5 µm. The other device parameters used for the simulation are shown in Table 1.

Table 1. Device parameters used during the simulation.

Parameter	Value
Doping concentration of Si layer	10^{12} cm^{-3}
Doping concentration of GaN buffer	10^{12} cm^{-3}
Doping concentration of GaN	10^{16} cm^{-3}

Table 1. *Cont.*

Parameter	Value
Doping concentration of AlGaN	10^{16} cm^{-3}
Doping concentration of P-GaN	2×10^{18} cm^{-3}
Gaussian doping concentration in the N-wells Peak concentration Characteristic length Peak position (from AlGaN/GaN interface)	 10^{19} cm^{-3} 0.05 µm 0.08 µm
Density of acceptor traps	10^{17} cm^{-3}
Energy of acceptor traps	0.368 eV
Source width W_S	2 µm
Source to gate distance W_{SG}	2 µm
Gate width W_G	2 µm
Gate to drain distance W_{GD}	5 µm
Drain width W_D	2 µm
Insulator thickness L_{INS}	10 nm
Barrier thickness (AlGaN) L_{B2}	30 nm
Interlayer thickness (AlN) L_{B1}	2 nm
Channel thickness (GaN) L_{Ch}	5 nm
Buried p-region thickness L_p	100 nm
Buffer thickness L_G	1 µm
Substrate thickness L_S	0.5 µm

2.3. Models

To predict the device's electrical characteristics, the TCAD simulator solved partial differential equations. The three main equations included Poisson's equation, the Continuity equation, and the drift–diffusion equation. In addition, several models were introduced to enhance the simulator's output. The Caughey and Thomas model was considered to account for the saturation velocity effect at high electric fields [46]. As shown in Equation (1), mobility is reduced as the electric field increases:

$$\mu_n(E) = \mu_{n0}\left[\frac{1}{1+\left(\frac{\mu_{n0}E}{VSAT}\right)^{BETA}}\right]^{\frac{1}{BETA}} \quad (1)$$

The values of the parameters used in Equation (1) are shown in Table 2. The values not mentioned in the table are taken from the default Silvaco library [47].

Table 2. Mobility parameters used during simulation.

Parameter	Value
μ_{n0} (GaN)	900 cm^2/V·s
μ_{n0} (AlGaN)	$300\,x + 900 \times (1 - x)$
μ_{n0} (2DEG)	1500 cm^2/V·s
VSATN (GaN)	2×10^7 cm/s
VSATN (AlGaN)	1.22×10^7 cm/s

Additional models incorporated in this study included Shockley–Read–Hall recombination and Fermi–Dirac statistics.

When simulating GaN-based HEMTs, the polarization field is crucial to the device's operation. Due to the discontinuity in the polarization field between the AlGaN and GaN layers, a positive charge will be created at the interface between the two materials. This positive charge will later attract electrons, causing the channel to form. In this work, due to the insertion of an AlN interlayer, the discontinuity of the polarization field was calculated twice: one at the AlGaN/AlN interface (σ_1) and another at the AlN/GaN interface (σ_2). To match the experimental results with the simulated ones, a fitting factor "K" was added when calculating σ_1 and σ_2:

$$\sigma_1 = (P_{sp}(AlN) - P_{sp}(Al_xGaN)) \times K \quad (2)$$

$$\sigma_2 = \left(P_{sp}(GaN) - P_{sp}(AlN) - P_{pz}(AlN)\right) \times K \quad (3)$$

Table 3 shows the device parameters and constants used during the simulation for this work.

Table 3. Device parameters and constants used in the simulation.

Parameter	Description	Value
K	Fitting factor	0.6
$P_{sp}(AlN)$	Spontaneous polarization (AlN)	-8×10^{-6} C/cm^2
$P_{sp}(GaN)$	Spontaneous polarization (GaN)	-2.9×10^{-6} C/cm^2
$P_{sp}(Al_xGaN)$	Spontaneous polarization (AlGaN)	$P_{sp}(AlN)x + P_{sp}(GaN)(1-x)$
$P_{pz}(Al_xGaN)$	Piezoelectric polarization (AlGaN)	$2\frac{a(0)-a(x)}{a(x)}\left(e_{31}(x) - e_{33}(x)\frac{c_{13}(x)}{c_{33}(x)}\right)$
$a(0)$	Lattice constant of GaN	3.189 Å
$a(x)$	Lattice constant of AlGaN	$3.112x + 3.189(1-x)$ Å
$e_{31}(x)$	Piezoelectric coefficients for AlGaN	$(-0.60 \times 10^{-4})x - (0.49 \times 10^{-4})(1-x)$ C/cm^2
$e_{33}(x)$		$(1.46 \times 10^{-4})x + (0.73 \times 10^{-4})(1-x)$ C/cm^2
$c_{13}(x)$	Elastic constants for AlGaN	$108x + 103(1-x)$ GPa
$c_{33}(x)$		$373x + 405(1-x)$ GPa

3. Results and Discussion

3.1. Effect of AlN in Conventional GaN MISHEMTs

First, we started by simulating the effect of including an AIN interlayer on the transfer characteristics of a conventional normally on GaN MISHEMT (without a buried p-region). The plot in Figure 3 shows the simulated drain current Id as a function of the gate voltage V_{gs}—$I_d(V_{gs})$ transfer characteristics—with and without an AlN interlayer. The transconductance gm was calculated and added to the figure based on Equation (4):

$$g_m = \frac{\partial Id}{\partial V_{gs}} \quad (4)$$

In line with the existing research [41,42], the inclusion of an AlN interlayer improves the device's current density by 8.43% (from 0.83 to 0.9 A/mm) while shifting the threshold voltage from −2.63 V to −3.75 V. Moreover, the maximum transconductance increased by 10% (from 0.139 to 0.153 S/mm). To explain this increase, the density of the 2DEGs at the AlGaN/GaN interface along the CUT in Figure 1 is shown in Figure 4 with and without the AlN interlayer. The inclusion of the AlN interlayer increased the 2DEG density by 67.44% (from 1.72×10^{19} cm^{-3} to 2.88×10^{19} cm^{-3}). The increase in 2DEG in the structure with an AlN interlayer occurs because, when AlN is grown on GaN, the significant lattice mismatch between the two layers causes a high stretch in the AlN layer. This stretching increases the piezoelectric polarization in AlN. Additionally, when compared to AlGaN, AlN exhibits higher spontaneous polarization. Together, these factors create a greater polarization field difference between the AlN and GaN layers, resulting in a higher bound charge at the

interface. As the bound charge increases, so does the 2DEG concentration, leading to higher current density and transconductance.

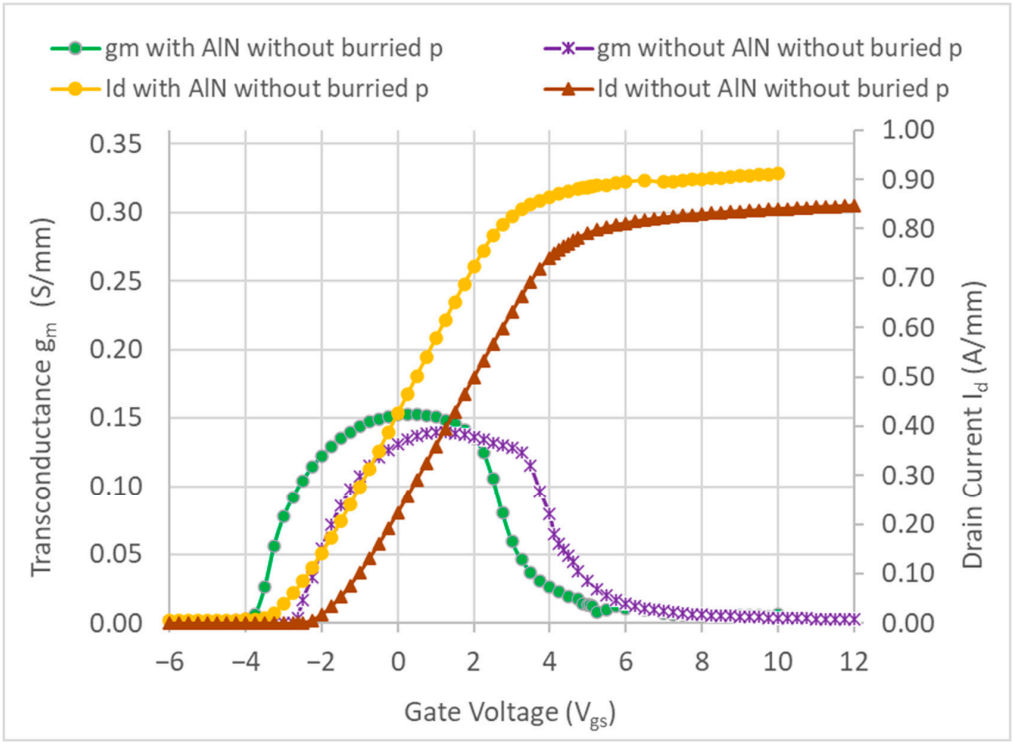

Figure 3. Drain current (I_d) and transconductance gm versus gate to source voltage (V_{gs}) characteristics for a conventional normally on MISHEMT with and without an AlN interlayer.

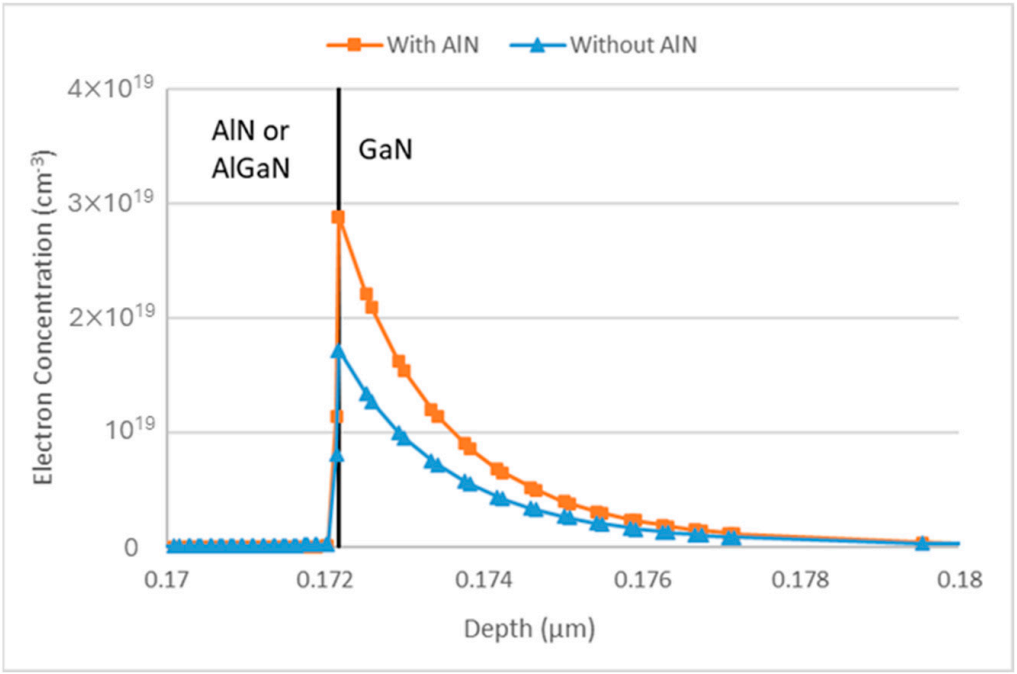

Figure 4. Density of 2DEGs at the AlGaN/GaN interface vs. AlN/GaN interface.

3.2. Effect of Buried p-Region in Conventional GaN MISHEMTs

The same study was applied to test the effect of the buried p-region in GaN MISHEMTs. The plot of Figure 5 represents the drain current Id as a function of the gate voltage

V_{gs}—$I_d(V_{gs})$ transfer characteristics—without an AlN interlayer, with and without a buried p-region.

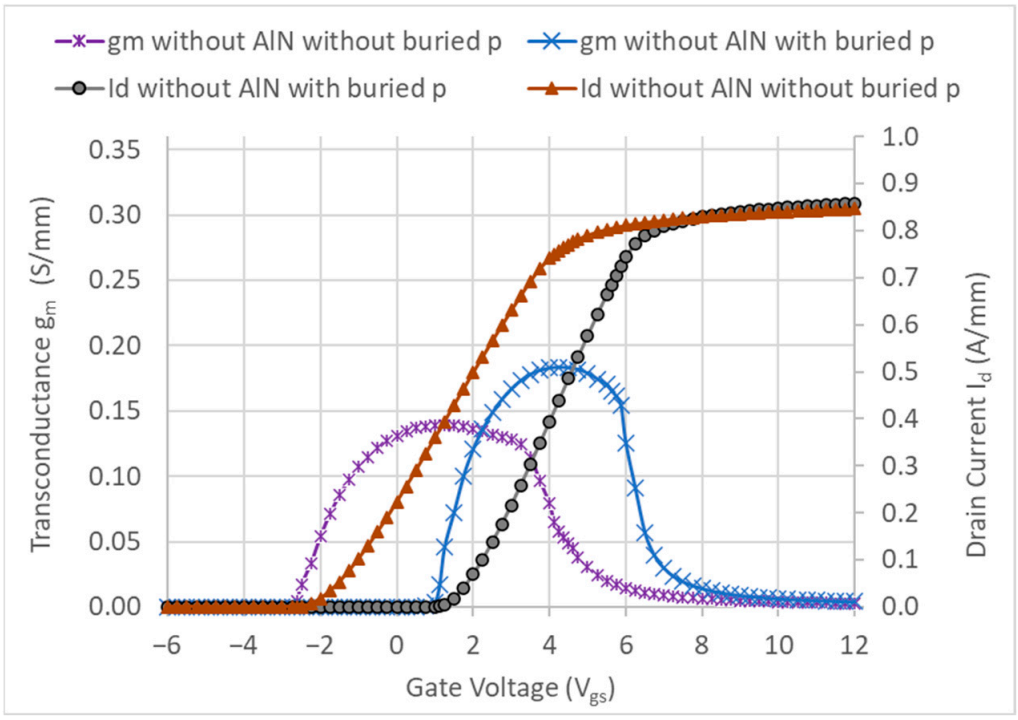

Figure 5. Drain current (I_d) and transconductance (gm) versus gate to source voltage (V_{gs}) for normally off HEMT with and without an AlN Interlayer.

Consistent with what is mentioned in [36], the threshold voltage shifts from −2.63 V to 1 V, resulting in the normally off operation. The reason behind the shift caused by the buried p-region can be explained by the conduction band profile along the cut in Figure 2. The profile is shown in Figure 6. The lift in the conduction band in the p-region causes the conduction band at the interface to rise. This rise depletes the channel electrons below the gate and, therefore, causes the normally off operation.

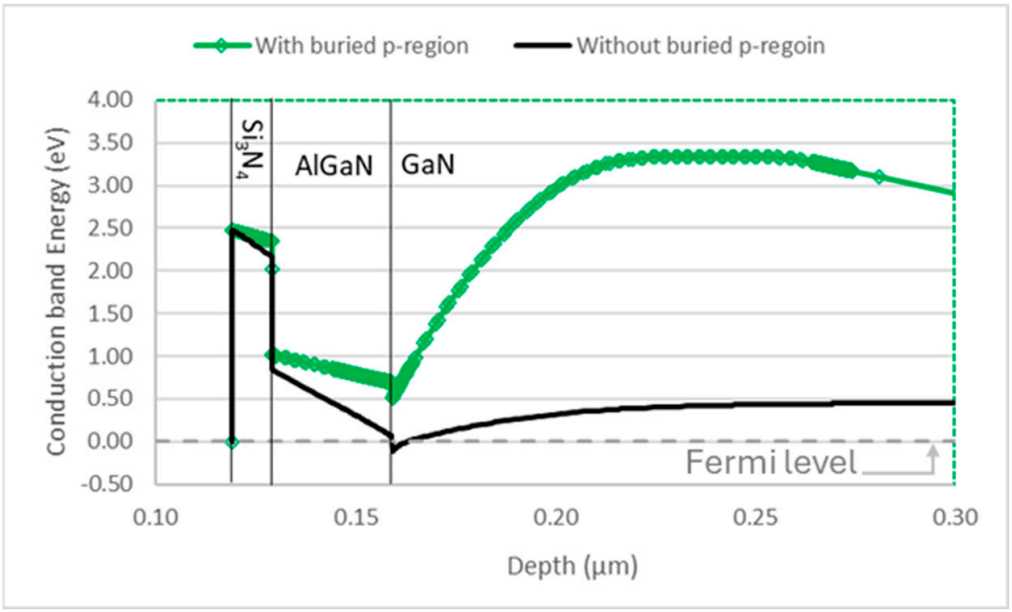

Figure 6. Conduction band along CUT in Figure 1 with and without a buried p-region.

3.3. Effect of AlN in Normally off MISHEMT with Buried p-Region

Figure 7 shows the plot of the drain current I_d as a function of the gate voltage V_{gs} for the normally off HEMT with a buried p-region with and without an interlayer, along with the transconductance.

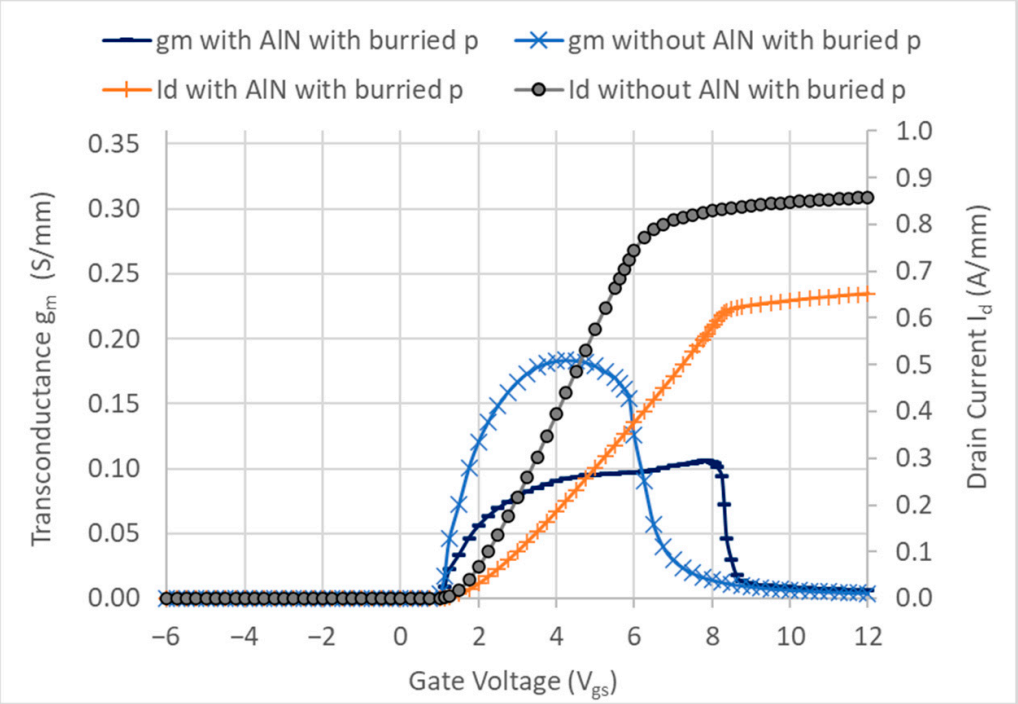

Figure 7. $I_d(V_{gs})$ transfer characteristics for the normally off HEMT with buried p-region with and without an AlN interlayer.

For the structure without AlN, the p-doping concentration in the p-region is 7.5×10^{17} cm^{-3}. However, for the structure with AlN, since the 2DEG density is higher, a higher p-doping concentration of 1.5×10^{18} cm^{-3} is required to achieve the same threshold voltage of 1 V. With the high increase in the p-doping concentration in the structure with AlN, the total current density of the device drops 21.83% (from 0.87 to 0.68 A/mm)

Moreover, a noticeable decrease in the transconductance was obtained when an interlayer was added with a higher p-doping concentration. The peak transconductance drops 44.4% (from 0.18 S/mm to 0.1 S/mm). To investigate this drop, the current density along the cut in Figure 2 with and without AlN is shown in Figure 8 at V_{gs} = 5 V and V_{ds} = 10 V. For the structure without AlN, at high gate voltages and due to the buried p-region, part of the current flows at the AlGaN/GaN interface, and another part flows near the insulator/AlGaN interface. The total current can be calculated as the area below the curve. On the other hand, when the AlN layer is added, the electrons are trapped at the AlGaN/GaN interface preventing additional current at the insulator/AlGaN interface. This blockage reduces the current density and the transconductance of the device.

Figure 9 shows the current density at different gate voltages for the structure with and without AlN. Without AlN, as the gate voltage increases, more electrons are attracted to the Si_3N_4/AlGaN interface and contribute to increasing the device's total current density. When AlN is added, channel electrons are trapped at the AlGaN/GaN interface and cannot migrate to the Si_3N_4 interface to further participate in the device's total current density.

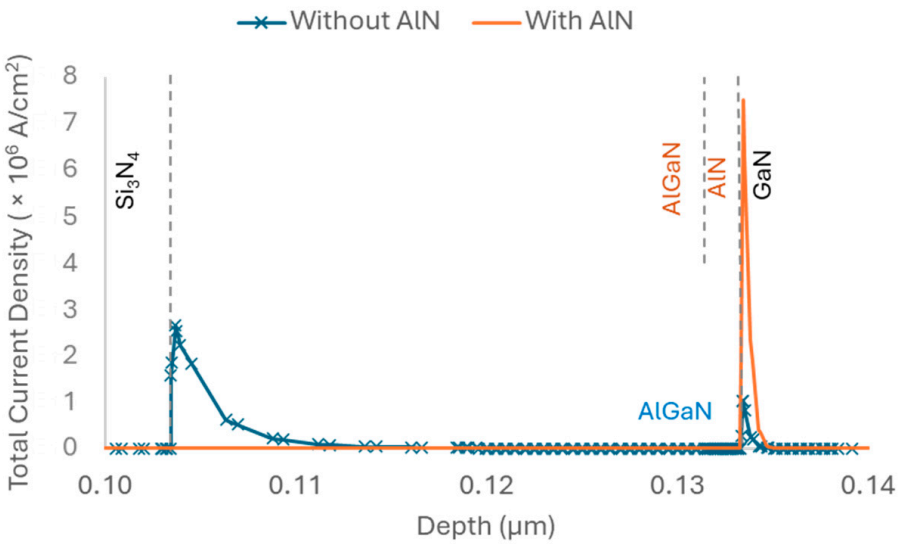

Figure 8. Total current density for the normally off HEMT with buried region with and without AlN at V_{gs} = 5 V and V_{ds} = 10 V.

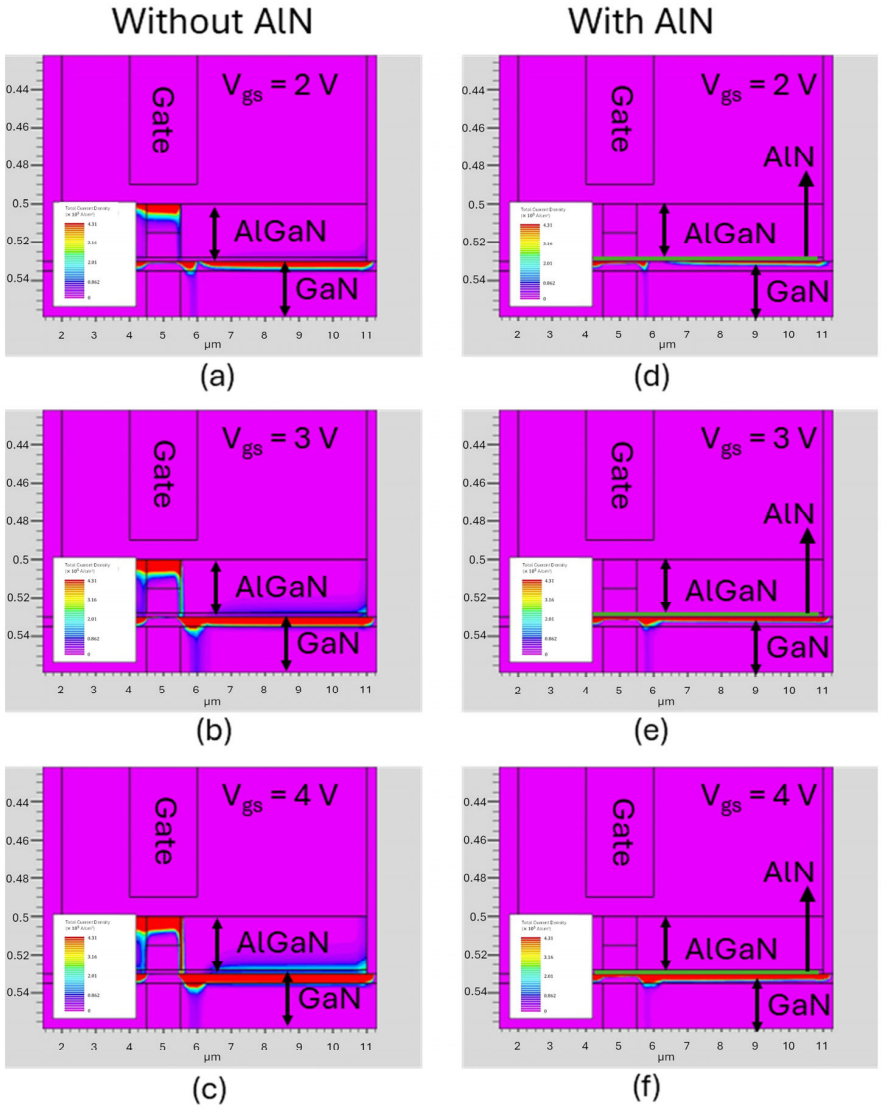

Figure 9. Total current density for the normally off HEMT with buried region at V_{ds} = 10 V with AlN at V_{gs} = (**a**) 2 V, (**b**) 3 V, and (**c**) 4 V and AlN at V_{gs} = (**d**) 2 V, (**e**) 3 V, and (**f**) 4 V, and V_{ds} = 10 V.

3.4. Limitations and Future Investigations

The mobility models implemented in this study successfully capture the electrical characteristics of both the normally on HEMT and the normally off HEMT with a buried p-region. However, since the output electrical characteristics are strongly mobility-dependent, changes in the structure and quality of the device layers, such as interface quality, defect density, and material purity, may affect the carrier mobility values and, consequently, alter device performance. Further experimental validation across different fabrication scenarios would be beneficial to comprehensively assess the relationship between the process conditions and device characteristics.

4. Conclusions

The introduction of AlN in conventional HEMTs is well-known for enhancing the current density and transconductance of the device. However, when applied to a normally off HEMT with a buried p-region, the effect is reversed. For the same threshold voltage, both the current density and transconductance decrease. This occurs because, at high p-doping concentrations beneath the gate electrode (under the AlGaN/GaN interface) and elevated gate voltages, electrons migrate to the insulator/AlGaN interface, contributing to the total conduction current. With the addition of the AlN layer, however, these electrons are trapped at the AlGaN/GaN interface and prevented from contributing elsewhere, resulting in a reduction in both current density and transconductance.

In the future, we aim to study the effect of AlN interlayers in normally off HEMTs with two p-regions: one buried below the AlGaN/GaN interface and another below the gate electrode.

Author Contributions: Conceptualization, S.H., B.B. and F.M.; methodology, S.H., B.B. and F.M.; software, S.H.; validation, S.H., B.B. and F.M.; formal analysis, S.H., B.B., and F.M.; investigation, S.H.; resources, F.M.; data curation, S.H.; writing—original draft preparation, S.H., B.B. and F.M.; writing—review and editing, S.H., B.B. and F.M.; visualization, S.H.; supervision, S.H., B.B. and F.M.; project administration, S.H., B.B. and F.M. All authors have read and agreed to the published version of the manuscript.

Funding: This research received no external funding.

Data Availability Statement: The original contributions presented in the study are included in the article. Further inquiries can be directed to the corresponding author.

Conflicts of Interest: The authors declare no conflicts of interest.

References

1. Dimarino, C.; Burgos, R.; Dushan, B. High-temperature silicon carbide: Characterization of state-of-the-art silicon carbide power transistors. *IEEE Ind. Electron. Mag.* **2015**, *9*, 19–30. [CrossRef]
2. Vobecký, J. The Current Status Of Power Semiconductors. *Facta Univ. Ser. Electron. Energy* **2015**, *28*, 193–203. [CrossRef]
3. Robles, E.; Matallana, A.; Aretxabaleta, I.; Andreu, J.; Fernández, M.; Martín, J.L. The role of power device technology in the electric vehicle powertrain. *Int. J. Energy Res.* **2022**, *46*, 22222–22265. [CrossRef]
4. Singh, R.; Pecht, M. Commercial impact of silicon carbide. *IEEE Ind. Electron. Mag.* **2008**, *2*, 19–31. [CrossRef]
5. Hu, J.; Zhang, Y.; Sun, M.-C.; Piedra, D.; Chowdhury, N.; Palacios, T. Materials and processing issues in vertical GaN power electronics. *Mater. Sci. Semicond. Process.* **2017**, *78*, 75–84. [CrossRef]
6. Nakagawa, A. Theoretical Investigation of Silicon Limit Characteristics of IGBT. In Proceedings of the 2006 IEEE International Symposium on Power Semiconductor Devices and IC's, Naples, Italy, 4–8 June 2006; pp. 1–4. [CrossRef]
7. Elasser, A.; Chow, T. Silicon carbide benefits and advantages for power electronics circuits and systems. *Proc. IEEE* **2002**, *90*, 969–986. [CrossRef]
8. Millán, J.; Godignon, P.; Perpiñà, X.; Pérez-Tomás, A.; Rebollo, J. A Survey of Wide Bandgap Power Semiconductor Devices. *IEEE Trans. Power Electron.* **2014**, *29*, 2155–2163. [CrossRef]

9. Rafin, S.M.S.H.; Ahmed, R.; Haque, M.A.; Hossain, M.K.; Haque, M.A.; Mohammed, O.A. Power Electronics Revolutionized: A Comprehensive Analysis of Emerging Wide and Ultrawide Bandgap Devices. *Micromachines* **2023**, *14*, 2045. [CrossRef] [PubMed]
10. Ozpineci, B. *Comparison of Wide-Bandgap Semiconductors for Power Electronics Applications*; Oak Ridge National Lab: Oak Ridge, TN, USA, 2004. [CrossRef]
11. Singhal, J.; Chaudhuri, R.; Hickman, A.; Protasenko, V.; Xing, H.G.; Jena, D. Toward AlGaN channel HEMTs on AlN: Polarization-induced 2DEGs in AlN/AlGaN/AlN heterostructures. *APL Mater.* **2022**, *10*, 111120. [CrossRef]
12. Diez, S.; Mohanty, S.; Kurdak, Ç.; Ahmadi, E. Record high electron mobility and low sheet resistance on scaled-channel N-polar GaN/AlN heterostructures grown on on-axis N-polar GaN substrates by plasma-assisted molecular beam epitaxy. *Appl. Phys. Lett.* **2020**, *117*, 042102. [CrossRef]
13. Lingaparthi, R.; Dharmarasu, N.; Radhakrishnan, K.; Ranjan, A.; Seah, T.L.A.; Huo, L. Source of two-dimensional electron gas in unintentionally doped AlGaN/GaN multichannel high-electron-mobility transistor heterostructures. *Appl. Phys. Lett.* **2021**, *118*, 122105. [CrossRef]
14. Saito, W.; Takada, Y.; Kuraguchi, M.; Tsuda, K.; Omura, I.; Ogura, T.; Ohashi, H. High breakdown voltage AlGaN-GaN power-HEMT design and high current density switching behavior. *IEEE Trans. Electron Devices* **2003**, *50*, 2528–2531. [CrossRef]
15. Lu, B.; Palacios, T. High Breakdown 1500 V AlGaN/GaN HEMTs by Substrate-Transfer Technology. *IEEE Electron Device Lett.* **2010**, *31*, 951–953. [CrossRef]
16. Pengelly, R.; Wood, S.; Milligan, J.; Sheppard, S.T.; Pribble, W. A Review of GaN on SiC High Electron-Mobility Power Transistors and MMICs. *IEEE Trans. Microw. Theory Tech.* **2012**, *60*, 1764–1783. [CrossRef]
17. Lyu, G.; Wang, Y.; Wei, J.; Zheng, Z.; Sun, J.; Zhang, L.; Chen, K.J. A Normally-off Copackaged SiC-JFET/GaN-HEMT Cascode Device for High-Voltage and High-Frequency Applications. *IEEE Trans. Power Electron.* **2020**, *35*, 9671–9681. [CrossRef]
18. Hamady, S.; Beydoun, B.; Morancho, F. A solution for channel electron migration in normally-off MIS-HEMT with buried fluorine ions. In Proceedings of the 2017 29th International Conference on Microelectronics (ICM), Beirut, Lebanon, 10–13 December 2017; pp. 1–4. [CrossRef]
19. Greco, G.; Iucolano, F.; Roccaforte, F. Review of technology for normally-off HEMTs with p-GaN gate. *Mater. Sci. Semicond. Process.* **2017**, *78*, 96–106. [CrossRef]
20. Huang, S.; Liu, X.; Wang, X.; Kang, X.; Zhang, J.; Bao, Q.; Wei, K.; Zheng, Y.; Zhao, C.; Gao, H.; et al. High Uniformity Normally-OFF GaN MIS-HEMTs Fabricated on Ultra-Thin-Barrier AlGaN/GaN Heterostructure. *IEEE Electron Device Lett.* **2016**, *37*, 1617–1620. [CrossRef]
21. Jiang, H.; Zhu, R.; Lyu, Q.; Tang, C.; Lau, K. Thin-barrier heterostructures enabled normally-OFF GaN high electron mobility transistors. *Semicond. Sci. Technol.* **2021**, *36*, 034001. [CrossRef]
22. Ostermaier, C.; Pozzovivo, G.; Carlin, J.-F.; Basnar, B.; Schrenk, W.; Douvry, Y.; Gaquiere, C.; DeJaeger, J.-C.; Cico, K.; Frohlich, K.; et al. Ultrathin InAlN/AlN Barrier HEMT with High Performance in Normally Off Operation. *IEEE Electron Device Lett.* **2009**, *30*, 1030–1032. [CrossRef]
23. Chakroun, A.; Jaouad, A.; Bouchilaoun, M.; Arenas, O.; Soltani, A.; Maher, H. Normally-off AlGaN/GaN MOS-HEMT using ultra-thin Al0.45Ga0.55N barrier layer. *Phys. Status Solidi A* **2017**, *214*, 1600836. [CrossRef]
24. Burnham, S.D.; Boutros, K.; Hashimoto, P.; Butler, C.; Wong, D.W.; Hu, M.; Micovic, M. Gate-recessed normally-off GaN-on- Si HEMT using a new O2-BCl3 digital etching technique. *Phys. Status Solidi C* **2010**, *7*, 2010–2012. [CrossRef]
25. Freedsman, J.; Watanabe, A.; Ito, T.; Egawa, T. Recessed gate normally-OFF Al2O3/InAlN/GaN MOS-HEMT on silicon. *Appl. Phys. Express* **2014**, *7*, 104101. [CrossRef]
26. Wu, J.; Lu, W.; Yu, P.K.L. Normally-OFF AlGaN/GaN MOS-HEMT with a two-step gate recess. In Proceedings of the 2015 IEEE International Conference on Electron Devices and Solid-State Circuits (EDSSC), Singapore, 1–4 June 2015; pp. 594–596. [CrossRef]
27. Liu, A.-C.; Tu, P.-T.; Chen, H.-C.; Lai, Y.-Y.; Yeh, P.-C.; Kuo, H.-C. Improving Performance and Breakdown Voltage in Normally-Off GaN Recessed Gate MIS-HEMTs Using Atomic Layer Etching and Gate Field Plate for High-Power Device Applications. *Micromachines* **2023**, *14*, 1582. [CrossRef] [PubMed]
28. Hamady, S.; Morancho, F.; Beydoun, B.; Austin, P.; Gavelle, M. A new concept of enhanced-mode GaN HEMT using fluorine implantation in the GaN layer. In Proceedings of the 2013 15th European Conference on Power Electronics and Applications (EPE), Lille, France, 2–6 September 2013; pp. 1–6. [CrossRef]
29. Hamady, S.; Morancho, F.; Beydoun, B.; Austin, P.; Gavelle, M. Scalable normally-off MIS-HEMT using fluorine implantation below the channel. In Proceedings of the 2014 International Symposium on Power Electronics, Electrical Drives, Automation and Motion, Ischia, Italy, 18–20 June 2014; pp. 124–127. [CrossRef]
30. Sun, N.; Huang, H.; Sun, Z.; Wang, R.; Li, S.; Tao, P.; Ren, Y.; Song, S.; Wang, H.; Li, S.; et al. Improving Gate Reliability of 6-In E-Mode GaN-Based MIS-HEMTs by Employing Mixed Oxygen and Fluorine Plasma Treatment. *IEEE Trans. Electron Device* **2022**, *69*, 82–87. [CrossRef]

31. Albany, F.; Curutchet, A.; Labat, N.; Lecourt, F.; Walasiak, E.; Maher, H. An Advanced Ageing Methodology for Robustness Assessment of Normally-off AlGaN/GaN HEMT. In Proceedings of the 2020 15th European Microwave Integrated Circuits Conference (EuMIC), Utrecht, The Netherlands, 10–15 January 2021; pp. 237–240.
32. Wang, H.-C.; Pu, T.; Li, X.; Liu, C.-H.; Wu, J.; Yang, J.; Zhang, Z.; Lu, Y.; Wang, Q.; Song, L.; et al. High-Performance Normally-Off Operation p-GaN Gate HEMT on Free-Standing GaN Substrate. *IEEE Trans. Electron Devices* **2022**, *69*, 4859–4863. [CrossRef]
33. He, J.; Xu, W.; Wang, F.; Ding, G.; Feng, Q.; Yu, P.; Wang, X.; Yu, C.; Zhang, Y.; Sun, R.; et al. 960V normally-off p-GaN gate HEMT with high threshold voltage and drain current. In Proceedings of the 2022 IEEE 16th International Conference on Solid-State & Integrated Circuit Technology (ICSICT), Nangjing, China, 25–28 October 2022; pp. 1–3. [CrossRef]
34. Rouly, D.; Tasselli, J.; Austin, P.; Haloui, C.; Isoird, K.; Morancho, F. Design Optimization of a New Nanostructured P-GaN Gate for Normally-off GaN HEMTs. In Proceedings of the 2022 29th International Conference on Mixed Design of Integrated Circuits and System (MIXDES), Wrocław, Poland, 23–24 June 2022; pp. 105–109. [CrossRef]
35. Sriramadasu, K.S.; Hsin, Y. Normally-Off p-GaN Gate AlGaN/GaN Transistor with a New Schottky Second Gate. *ECS J. Solid State Sci. Technol.* **2022**, *11*, 105004. [CrossRef]
36. Hamady, S.; Morancho, F.; Beydoun, B. Localized buried P-doped region for E-mode GaN MISHEMTs. *J. Comput. Electron.* **2023**, *22*, 190–198. [CrossRef]
37. Chapelle, A.; Frayssinet, É.; Cordier, Y.; Spiegel, Y.; Benmosfeta, L.; Trémouilles, D.; Isoird, K. Première démonstration expérimentale d'un interrupteur HEMT normally-off en GaN avec une région P-GaN enterrée. In *Symposium de Génie Electrique*; Université de Lorraine: Nancy, France, 2018; pp. 3–5.
38. Liu, K.; Wang, C.; Zheng, X.; Ma, X.; Zhang, K.; Zhang, W.; Bai, J.; Li, A.; Hao, Y. Ultra-Low Gate Leakage Current and Enhanced Gate Reliability in p-GaN HEMT with AlN/GaN/AlN Double Barriers Cap Layer. *IEEE Electron Device Lett.* **2024**, *45*, 1736–1739. [CrossRef]
39. Kotani, J.; Yaita, J.; Homma, K.; Ozaki, S.; Yamada, A.; Sato, M.; Ohki, T.; Nakamura, N. 24.4 W/mm X-Band GaN HEMTs on AlN Substrates with the LPCVD-Grown High-Breakdown-Field SiNx Layer. *IEEE J. Electron Devices Soc.* **2023**, *11*, 101–106. [CrossRef]
40. Miyoshi, M.; Tanaka, S.; Kawaide, T.; Inoue, A.; Egawa, T. DC and Pulse I–V Characteristics of Strain-Engineered AlGaInN/GaN HEMTs fabricated on Single-Crystal AlN Substrate. *Phys. Status Solidi A* **2023**, *220*, 2200733. [CrossRef]
41. Douara, A.; Rabehi, A.; Baitiche, O. Impact of AlN interlayer on the electronic and I-V characteristics of In0.17Al0.83N/GaN HEMTs devices. *Rev. Mex. Física* **2023**, *69*, 031602-1. [CrossRef]
42. Lee, T.; Hieu, L.T.; Chiang, T.-H.; Lee, C.; Lin, C.-H.; Chang, E.Y. High-Quality AlGaN/GaN HEMTs Growth on Silicon Using Al0.07Ga0.93N as Interlayer for High RF Applications. *ECS J. Solid State Sci. Technol.* **2023**, *12*, 105002. [CrossRef]
43. Roy, P.; Jawanpuria, S.; Vismita; Prasad, S.; Islam, A. Characterization of AlGaN and GaN Based HEMT with AlN Interfacial Spacer. In Proceedings of the 2015 Fifth International Conference on Communication Systems and Network Technologies, Gwalior, India, 4–6 April 2015; pp. 786–788. [CrossRef]
44. Shrestha, N.M.; Wang, Y.Y.; Li, Y.; Chang, E.Y. Simulation Study of AlN Spacer Layer Thickness on AlGaN/GaN HEMT. *Himal. Phys.* **2013**, *4*, 14–17. [CrossRef]
45. Miyoshi, M.; Egawa, T.; Ishikawa, H. Study on mobility enhancement in MOVPE-grown AlGaN/AlN/GaN HEMT structures using a thin AlN interfacial layer. *Solid-State Electron.* **2006**, *50*, 1515–1521. [CrossRef]
46. Caughey, D.M.; Thomas, R.E. Carrier mobilities in silicon empirically related to doping and field. *Proc. IEEE* **1967**, *55*, 2192–2193. [CrossRef]
47. SILVACO. *ATLAS User's Manual Device Simulation Software*; SILVACO: Santa Clara, CA, USA, 2011; pp. 330–331.